Generalized Response Spectrum Analysis for Structures with Dampers

Yuki Terazawa[a] **and Toru Takeuchi**[a]

In this study, a computational seismic design routine is proposed based on a generalized response spectrum analysis for highly indeterminate structures with energy-dissipation members, such as viscous or elasto-plastic dampers. Complex stiffness terms are introduced to account for displacement-dependent damping, and a three-dimensional (3-D) element stiffness matrix with complex axial stiffness is proposed for elasto-plastic dampers. A modified complete quadratic combination method previously developed for real symmetric damped systems is extended to complex asymmetric damped systems, based on a theoretical analysis of eigenvalue equations. The response is evaluated by iteratively conducting complex eigenvalue analysis and modal combination. The accuracy is confirmed through comparison to nonlinear response history analysis of 2-D frame models. Finally, an example application is presented of a 3-D truss tower seismically retrofitted by replacing the braces with viscoelastic and then elasto-plastic dampers. The proposed design routine is used to rapidly identify novel and efficient damper arrangements and sizing distributions, avoiding computationally intensive nonlinear response history analysis. [DOI: 10.1193/092217EQS188M]

INTRODUCTION

Response spectrum analysis (RSA) is a computationally efficient method to determine the seismic response of frame structures, but as a linear method is less capable of analyzing structures with dampers, which generally require nonlinear response history analysis (NLRHA). One technique to overcome this limitation is to employ equivalent linear damping (Jacobsen 1930), which has been applied with RSA to evaluate the response reduction effect of dampers in passively controlled structures (e.g., Fu and Kasai 1998, Kasai et al. 2009). Equivalent damping rules have been established for viscous, viscoelastic (VE), and elasto-plastic (EP) energy-dissipation devices mounted in moment frames, as well as design procedures for single- and multiple-degree-of-freedom systems (SDOF or MDOF) (e.g., JSSI 2013, AIJ 2016). Recently, energy-dissipation devices have been applied to innovative, passively controlled systems such as rocking frames, spine frames, and damped outrigger systems. For each system, simplified models and design procedures have been proposed (Eatherton et al. 2014, Takeuchi et al. 2015, Huang and Takeuchi 2017). While these non-computational design procedures are practical for design, analysis limitations make it is necessary to confirm the final response using NLRHA, with the process iterated until a satisfactory design is achieved. While sufficient for typical or simple cases, this is not necessarily an efficient process for highly indeterminate structures, where an efficient damper distribution may not be

[a] Department of Architecture and Building Engineering, Tokyo Institute of Technology, Tokyo, Japan; Email: terazawa.y.aa@m.titech.ac.jp (YT, corr. author)

Earthquake Spectra, Volume 34, No. 3, pages 1459–1479, August 2018;

immediately apparent. In these cases, it is useful to apply generative computational methods to help explore the design space. However, in a fast-paced design environment, the time required for NLRHA makes this unwieldy if a large number of analysis runs is required. Thus, it is desirable to use RSA, but the increased damping introduced by energy dissipation devices must be accurately modeled.

Several approximate methods to evaluate the modal damping ratios have previously been proposed. An approximation for MDOF models that is suitable for hand calculation was proposed by Biggs and Whitman (1970) and used in the substitute structure method (Shibata and Mete 1976). This extended equivalent approach is adopted in the Japanese passive control design manual (JSSI 2013) for a variety of damper types. Warburton and Soni (1977) proposed an approximate method using undamped modal analysis and a corresponding damping matrix, which is accurate for moderately nonlinear structures. Takeuchi et al. (2015) applied the Biggs rule to three-dimensional (3-D) structures with VE dampers arranged as braces, and demonstrated its efficiency in combination with a genetic optimization algorithm. However, in these methods, modal combination responses are evaluated based on the undamped mode shapes, giving no guarantee that the results are accurate for large equivalent damping ratios, which poses a limitation. In the previous study, the first mode damping ratios of validation models never exceeded 7%. As one solution to this issue, Sinha and Igusa (1995) extended the square root of the sum of squares (SRSS) and complete quadratic combination (CQC) rules to systems with non-proportional damping. This "modified CQC" method is particularly attractive, as it can consider phase effects among different modes and is reasonably accurate for up to 35% viscous damping when compared to an approximate modal analysis using undamped mode shapes. While this method is sufficient for viscous and VE damping, it is not appropriate for displacement-dependent damping generated from elasto-plastic devices.

In this study, EP damping is modeled using complex stiffness terms (Myclestad 1952), which is an approach often applied when conducting modal response analysis using Fourier transformations for other dynamics problems (Bae et al. 2014, Shirai and Inoue 2014). Complex stiffness simulates damping using a phase lag between a real and imaginary part in the element stiffness matrix, providing a good estimate of the effect of displacement-dependent damping. Ishimaru and Chunhuan (2015) modeled EP dampers using complex stiffness, but used an EP response spectrum calibrated for a specific hysteresis and the SRSS rule with absolute values of the complex participation vectors. Greater accuracy may be obtained by extending the modified CQC method, which was developed for real symmetric damped systems, to complex asymmetric damped systems. For practical designs using an elastic response spectrum, both viscous and EP damping should be considered, with the latter incorporated as complex stiffness.

The objective of this study is to develop a generic computational RSA routine that can be applied to 3-D frame models with both viscous and EP energy-dissipation devices. This offers the possibility of applying flexible computational optimization routines as a design tool to generate efficient damper distributions, using the proposed RSA method for the analysis. In this study, a particular emphasis is placed on EP dampers arranged in a brace configuration, e.g., buckling-restrained braces. A 3-D element stiffness matrix with complex axial stiffness terms for EP dampers is proposed and several equivalent damping formulations compared. The accuracy and limitations are then examined using NLRHA of

2-D frames of various heights, stiffness ratios, damper arrangements, and damper yield ratios. Finally, an example is presented applying the proposed method to a 3-D model of a truss tower with VE and EP dampers. This is based on a structure constructed in Japan that was previously retrofitted with buckling restrained braces (Ookouchi et al. 2005).

SUMMARY OF PREVIOUS RSA METHODS

This chapter summarizes previous RSA methods for MDOF structures with energy-dissipation elements that are of relevance to the proposed method, including the complex stiffness approach. Hereafter, the real symmetric mass matrix, real symmetric damping matrix, real symmetric stiffness matrix, and complex asymmetric stiffness matrix are denoted "**M**," "**C**," "**K**," and "$\mathbf{K_{eq}}$," respectively, and the corresponding systems are denoted "**MK**," **MCK**," "$\mathbf{MK_{eq}}$" or "$\mathbf{MCK_{eq}}$," respectively.

EXTENDED EQUIVALENT LINEAR APPROACH

The equivalent modal damping ratio ξ_s^i at the i^{th} story or member in the s^{th} mode is calculated. The equivalent modal damping ratio ξ_s^{eq} in Equation 1 is obtained for the s^{th} mode using the weighted average of the modal elastic strain energies W_s^i (Biggs and Whitman 1970):

$$\xi_s^{eq} = \frac{\sum_i \xi_s^i W_s^i}{\sum_i W_s^i} = \frac{1}{4\pi}\frac{\sum_i E_s^i}{\sum_i W_s^i} \tag{1}$$

This average value is equal to the equivalent damping ratio calculated from a direct summation of the elastic strain energy W_s and dissipated energy E_s under a steady-state response. Therefore, Equation 1 is an extension of the original SDOF equivalent linear approach (Jacobsen 1962). In previous work (Takeuchi et al. 2015), this approach was applied to a truss structure with VE dampers. However, this approach assumes undamped mode shapes, which may significantly differ from the damped mode shapes when the equivalent supplemental damping is large. Furthermore, the degree(s) of freedom used to compute the elastic strain energy W_s depends on the building type, which poses a challenge for highly indeterminate structures.

EXTENDED MODAL COMBINATION METHOD FOR NON-PROPORTIONAL DAMPING

Complex eigenvalue analysis is suitable for computing the exact modal damping ratios and damped mode shapes, including phase effects. However, as indicated by Equation 2, the decoupled modal equation obtained from the first-order simultaneous differential equations (Foss 1958) include complex terms related to displacement and velocity. Thus, this cannot be directly applied in a conventional RSA:

$$\dot{{}_iq_s} - \lambda_{si}{}_iq_s = -\beta_{s\ddot{u}g} \tag{2}$$

where ${}_iq_s$ is the s^{th} complex function of the i^{th} global DOF, λ_s is the s^{th} complex eigenvalue, β_s is the s^{th} complex participation factor, and $\ddot{u}_g$ is the ground acceleration.

Sinha and Igusa (1995) proposed an approximate formula to apply complex eigenvectors to RSA. In a real symmetric damped system (type **MCK**), a physical displacement y_s

associated with the s^{th} mode is provided, and Equation 3 is assumed based on the conjugate property. Equation 4 is obtained by substituting Equation 3 into Equation 2, and the maximum response is calculated from the elastic response spectrum:

$$ {}_i q_{s0}/\beta_s = -\lambda_s^* {}_i y_s + {}_i \dot{y}_s \tag{3} $$

$$ {}_i \ddot{y}_s + 2\xi_s \omega_s {}_i \dot{y}_s + \omega_s^2 {}_i y_s = -\ddot{u}_g, \quad \max|y_s| = S_d(\omega_s, \xi_s) \tag{4} $$

where * is the conjugate property, ω_s is the natural circular frequency of the s^{th} mode, and S_d is the spectral displacement.

From a summation of Equation 3, the total modal displacement is given by Equation 5. The absolute value for the i^{th} DOF of the real-valued participation vector ${}_i B_s$ and approximate phase angle ${}_i \theta_s$ is obtained from Equation 6:

$$ U(t) = 2 \sum_{s=1}^{n} \{ -\mathrm{Re}(\lambda_s^* \beta_{si} \phi_s) {}_i y_s + \mathrm{Re}(\beta_{si} \phi_s) {}_i \dot{y}_s \} \approx {}_i B_s S_d(\omega_s, \xi_s) \sin(\omega_s t + {}_i \theta_s) \tag{5} $$

where

$$ {}_i B_s = 2|\mathrm{Re}(\lambda_s^* \beta_{si} \phi_s) / \sin({}_i \theta_s)|, \quad {}_i \theta_s = \tan^{-1}(-\mathrm{Re}(\lambda_s^* \beta_{si} \phi_s) / \mathrm{Re}(\beta_{si} \phi_s)) \tag{6} $$

${}_i \phi_s$ is the complex eigenvector value for the i^{th} DOF of the s^{th} mode.

The combined modal displacements response ${}_i R_{\text{CQC}}$ for the i^{th} DOF is calculated in Equation 7 from the modal participation B, phase angle θ, modal correlation coefficient ρ (from the original CQC method), and spectral displacement S_d. Note that this can consider phase effects for cases involving high damping, and Equations 5 to 7 are calculated for each DOF in the system.

$$ {}_i R_{\text{CQC}} = \sqrt{\sum_{s=1}^{n} \sum_{r=1}^{n} {}_i B_{si} B_r S_{d_s} S_{d_r} \cos({}_i \theta_s - {}_i \theta_r) \rho_{sr}} \tag{7} $$

As mentioned previously, the modified CQC method is valid for real symmetric damped systems. In the following section, this method is extended to systems with displacement-dependent supplementary damping, such as those with EP dampers.

RESPONSE EVALUATION FOR COMPLEX ASYMMETRIC DAMPED SYSTEM

Here, complex stiffness is used to simulate EP damping. Complex stiffness provides a good estimate of displacement-dependent damping compared to other approaches that translate elasto-plasticity into equivalent viscoelasticity, where frequency-dependent damping affects higher-mode damping ratios. The modified CQC method is of interest, as this calculation features conjugate pairs of complex eigenvalues. In the proposed routine, a complex asymmetric damped system (including both a real valued damping matrix $\mathbf{C}$ and complex stiffness matrix $\mathbf{K_{eq}}$) is applied, iterating to obtain the complex eigenvalues and mode shapes. Subsequently, the real valued modal and combined CQC response are evaluated using the conjugate property and Equations 2 to 7. Note that this procedure converts the complex

modal response to one of a real symmetric damped system, which has a defined elastic response spectrum.

The free vibration equation for a SDOF $\mathbf{MCK_{eq}}$ system is given by Equation 8:

$$m\ddot{x} + c\dot{x} + (a + ib\mathrm{sgn}\omega_e)k_0 x = 0, \quad a > 0, b \geq 0 \tag{8}$$

where m is the mass, c is the viscous damping coefficient, k_0 is the initial elastic stiffness, i is the imaginary unit, a is the real part and b the imaginary part of the complex stiffness, and ω_e is the circular excitation frequency.

Reformulating Equation 8, the characteristic equation is obtained from Equation 9. Neglecting repeated roots, the complex eigenvalue group is obtained from Equation 10:

$$\lambda^2 + 2\xi_v\omega_0\lambda + (a + ib\mathrm{sgn}\omega_e)\omega_0^2 = 0, x = Ae^{\lambda t} \tag{9}$$

$$\lambda = \begin{cases} \begin{cases} -(\xi_v + \xi_k)\omega_0 + i\sqrt{(a - \xi_v^2) + \xi_k^2}\omega_0 \\ -(\xi_v - \xi_k)\omega_0 - i\sqrt{(a - \xi_v^2) + \xi_k^2}\omega_0 \end{cases} & (\omega_e > 0) \\ \begin{cases} -(\xi_v + \xi_k)\omega_0 - i\sqrt{(a - \xi_v^2) + \xi_k^2}\omega_0 \\ -(\xi_v - \xi_k)\omega_0 + i\sqrt{(a - \xi_v^2) + \xi_k^2}\omega_0 \end{cases} & (\omega_e < 0) \end{cases} \tag{10}$$

Here

$$\xi_k = \sqrt{\frac{-(a - \xi_v^2) + \sqrt{(a - \xi_v^2)^2 + b^2}}{2}} \tag{11}$$

ω_0 is the natural circular frequency, ξ_v is the damping ratio (related only to viscous damping), ξ_k is the damping ratio related to the complex stiffness (but including a viscous damping component), and A is the displacement amplitude, which is an unknown.

Note that Equation 10 is a generalized eigenvalue expression, reducing to that of the **MCK** system when the parameter b is set to zero, the $\mathbf{MK_{eq}}$ system when damping c is set to zero (as given in Equation 12), and the **MK** system when both parameter b and damping c are set to zero:

$$\lambda = \begin{cases} \begin{cases} -\sqrt{\frac{-a+\sqrt{a^2+b^2}}{2}}\omega_0 + i\sqrt{\frac{a+\sqrt{a^2+b^2}}{2}}\omega_0 \\ +\sqrt{\frac{-a+\sqrt{a^2+b^2}}{2}}\omega_0 - i\sqrt{\frac{a+\sqrt{a^2+b^2}}{2}}\omega_0 \end{cases} & (\omega_e > 0) \\ \begin{cases} -\sqrt{\frac{-a+\sqrt{a^2+b^2}}{2}}\omega_0 - i\sqrt{\frac{a+\sqrt{a^2+b^2}}{2}}\omega_0 \\ +\sqrt{\frac{-a+\sqrt{a^2+b^2}}{2}}\omega_0 + i\sqrt{\frac{a+\sqrt{a^2+b^2}}{2}}\omega_0 \end{cases} & (\omega_e < 0) \end{cases} \tag{12}$$

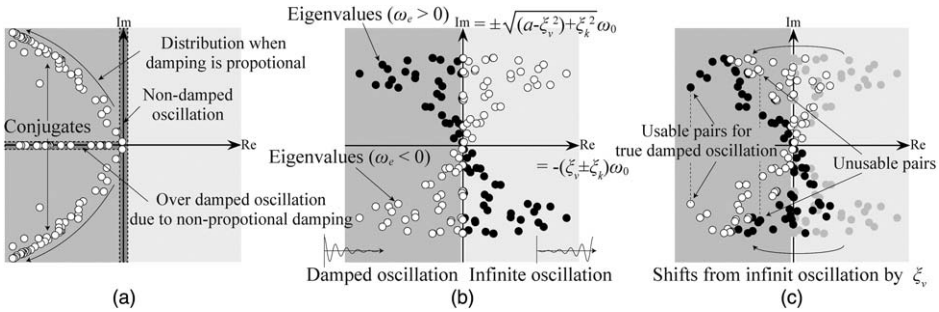

Figure 1. Example eigenvalue distribution, including complex stiffness: (a) Type MCK; (b) type MK_{eq}; and (c) type MCK_{eq}.

The eigenvalue distributions for the generalized and simplified systems are visualized in Figure 1, calculated from a 3-D tower model presented later. This model includes both proportional viscous damping and EP dampers that are represented as complex stiffness. In this system, complex stiffness is a fictional expression representing displacement-dependent damping, and sgnω_e is the signum function to account for the phase lag and conjugate property of the asymmetric damped **MCK** system (Figure 1a). As shown in Equation 12 and Figure 1b, by employing the signum function, it is easy to extract each mode group for the $\mathbf{MK_{eq}}$ system due to symmetry. Modal response analysis of these simplified systems uses both symmetric eigenvalues, including the negative real parts (e.g. Bae et al. 2014, Shirai and Inoue 2014). However, in $\mathbf{MCK_{eq}}$ systems, the axes of symmetry are dependent on the viscous damping ξ_v of each mode, and some eigenvalues (related to infinite oscillations in $\mathbf{MK_{eq}}$) shift to quadrants corresponding to damped oscillations, as shown in Figure 1c. This lack of symmetry would normally make it impossible to directly extract the modal parameters (ξ_v, ξ_k, ω_0). Nevertheless, the true damped oscillations may still be obtained by identifying appropriate conjugate pairs, such as the pair given by the first and third lines of Equation 10. This conjugate property is an essential feature of the modified CQC method, and permits the modal response of $\mathbf{MCK_{eq}}$ systems to be determined from a conventional **MCK** elastic response spectra. In the proposed routine, the pairs mentioned above are applied to Equations 2 to 7, with the equivalent **MCK** system s^{th} mode's natural circular frequency ξ_s and modal damping ratio ω_s calculated from Equation 13:

$$\omega_s = |\lambda_s|, \xi_s = -\mathrm{Re}(\lambda_s)/\omega_s \tag{13}$$

COMPLEX STIFFNESS FOR ELASTO-PLASTIC DAMPERS

ELEMENT STIFFNESS MATRIX

A central aspect of the proposed procedure is the concept that EP damping may be represented as a complex element stiffness term. The general 3-D complex stiffness matrix for a beam-column element is presented in Equation 14. Three displacement DOFs (u_x, u_y, u_z) and three rotational DOFs (θ_x, θ_y, θ_z) are included at each end, the x direction of the local coordinate system corresponds to the element axial direction, and the member is assumed to be

prismatic. Complex stiffness is assigned t only o the axial terms in the linear stiffness matrix K_L, with the bending terms primarily included to model non-damper elements and to avoid numerical singularities in a 3-D model. The geometric stiffness matrix K_G is constructed as a real symmetric matrix after application of dead loads, accounting for compression softening effects. This equivalent linearized element stiffness matrix K_{eq} models axial yielding dampers in a brace or axial configuration, but not dampers that yield in flexure. Note that the complex stiffness terms are included only with the proposed RSA routine, but are excluded if conducting a validation analysis using NLRHA:

$$K_{eq} = K_L + K_G = \begin{pmatrix} k_x & \cdots & -k_x & \cdots \\ \vdots & \ddots & \vdots & \ddots \\ -k_x & \cdots & k_x & \cdots \\ \vdots & \ddots & \vdots & \ddots \end{pmatrix} + K_G, k_x = (a + ib\,\mathrm{sgn}\omega_e)\frac{A_b E}{L_b} \tag{14}$$

where A_b is the section area, E is Young's modulus, and L_b is the member length.

PARAMETER FORMULATIONS

The dotted lines in Figure 2 show the normalized bilinear load–deformation relationship of an EP damper under steady-state response. As discussed in previous studies (e.g., Jennings 1963), the equivalent linear approach can readily accommodate any EP hysteresis rule, as compared with the original frequency-dependent damping formulation. The complex stiffness formulation can be similarly adapted to model arbitrary hysteresis rules using the coefficients a and b. In this paper, three well-known formulations for the equivalent damping of the bilinear hysteresis rule are presented, which target the same displacement A as the original bilinear hysteresis loop, as shown in Figure 2. In these equations, μ is the ductility, p is the ratio of post-yield to initial stiffness, and ξ' is the element damping ratio. The equivalent secant stiffness ratio γ_K, corresponding to the maximum deformation U_m and normalized energy dissipation ratio γ_E, are calculated from Equation 15. In this study, p is defined

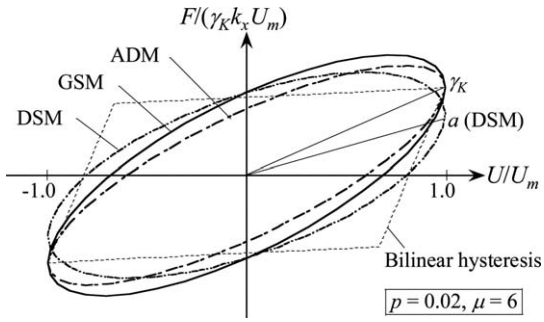

Figure 2. Normalized load–deformation relationship under a steady-state response.

Table 1. List of parameter formulations for elasto-plastic bilinear hysteresis

Method series	a	b	ξ'	Reference
Geometrical stiffness method (GSM)	γ_K	γ_E	$\frac{\gamma_E}{2\gamma_K}$	Jacobsen (1962)
Average damping method (ADM)	γ_K	$2\gamma_K h$	$\frac{1}{\mu}\int\frac{\gamma_E}{2\gamma_K}$	Newmark and Rosenblueth (1971)
Dynamic stiffness method (DSM)	$\frac{1-p}{\pi}\left\{\cos^{-1}\left(1-\frac{2}{\mu}\right)-\left(1-\frac{2}{\mu}\right)\frac{2}{\mu}\sqrt{\mu-1}\right\}+p$	γ_E	$\frac{b}{2a}$	Caughey (1960)

as 0.02, and the expected yield strength is defined as $225\,\mathrm{N/mm^2}$ assuming steel grade LY225 (Japanese damper steel).

$$\gamma_K = \frac{1+p(\mu-1)}{\mu},\quad \gamma_E = \frac{4}{\pi}\frac{(1-p)(\mu-1)}{\mu^2} \tag{15}$$

Table 1 presents the equivalent linearization formulations. The geometrical stiffness method (GSM), in which the real part of the stiffness is set as the equivalent stiffness, and where the energy dissipation under one cycle of sinusoidal excitation is equal to that of the original hysteresis, corresponds to a traditional equivalent linear approach (Jacobsen 1962). The average damping method (ADM) corresponds to the average damping concept proposed by Newmark and Rosenblueth (1971), which is often recommended in design manuals (e.g., JSSI 2013). This assigns ξ' as the average equivalent damping computed from a ductility of 1 to μ, providing a better approximation of the random amplitudes experienced in real ground motions. This produces a more conservative damping ratio than GSM, as indicated by a smaller enclosed loop area in Figure 2. The dynamic stiffness method (DSM) uses the first approximation of the Fourier series for the bilinear hysteresis proposed by Caughey (1960). The real part of the complex stiffness is generally less than γ_K. This approach is included in the Japanese design recommendations (AIJ 2016), and is used to analyze the steady state response of seismically isolated buildings. In this study, the real valued participation vector used to display the mode shape and evaluate modal deformations is calculated from Equation 16:

$${}_iB'_s = {}_iB_s \mathrm{sgnRe}(\beta_{si}\phi_s) \tag{16}$$

COMPUTATIONAL ROUTINE

The flowchart for the proposed RSA routine, which this paper refers to as "generalized RSA" (GRSA), is outlined in Figure 3. This is intended to be applied to structural models consisting of an elastic main structure and discrete energy-dissipation braces.

First, the initial elastic CQC displacement vector $\{\delta_0\}$ is computed using RSA of a conventional **MCK** system. For this stage, the vibration system includes only the proportional damping matrix and any supplemental viscous dampers, and the complex stiffness

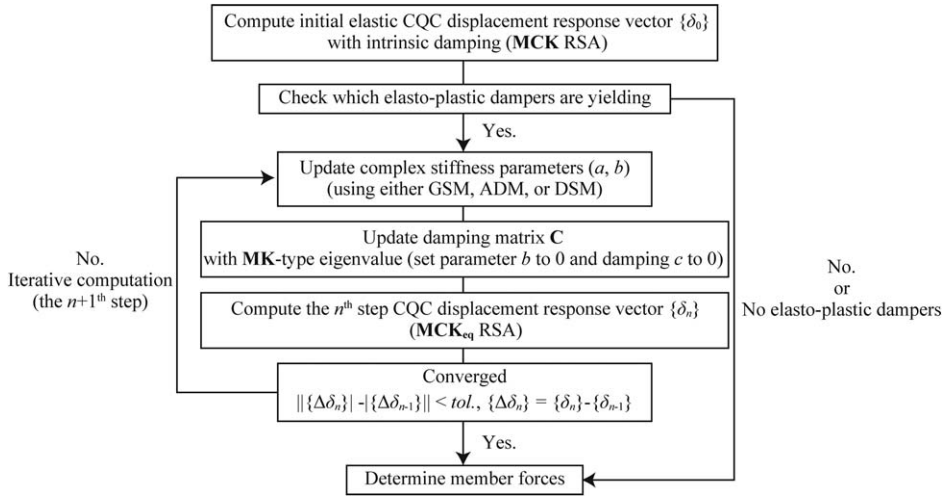

Figure 3. Flowchart of generalized RSA routine.

parameters a and b are set to one and zero, respectively. Second, the combined CQC response is calculated to determine which, if any, EP dampers have exceeded their yield displacements. The complex stiffness terms are calculated from Table 1 using the initial estimate of ductility demands for all yielding dampers. Third, the n^{th} step CQC displacement vector $\{\delta_n\}$ is computed using RSA of a $\mathbf{MCK_{eq}}$ system. The $\mathbf{MCK_{eq}}$ CQC response is then iteratively calculated, updating the complex stiffness terms based on the revised ductility until displacement convergence is achieved (Equation 17). This update process is similar to the substitute structure approach. Note that the proportional or non-proportional damping matrix is updated using the real symmetric stiffness matrix, including only the parameter a and the real eigenvalue analysis from the current iteration. In this study, convergence was generally achieved within 10 iterations. Finally, the combined response is evaluated, including element forces.

$$\left|\,|\{\Delta\delta_n\}| - |\{\Delta\delta_{n-1}\}|\,\right| < tol., \quad \{\Delta\delta_n\} = \{\delta_n\} - \{\delta_{n-1}\} \tag{17}$$

Response spectra corresponding to major damping ratios may be prepared in advance, and then adjusted to the precise modal damping ratio ξ_s using the damping adjustment factor D_h, as given by Equation 18:

$$S_d(\xi_s,\omega_s) = D_h \frac{S_a(\xi_0,\omega_s)}{\omega_s^2}, \quad D_h = \sqrt{\frac{1+\alpha\xi_0}{1+\alpha\xi_s}} \tag{18}$$

where ξ_0 is the damping ratio of the preset table close to the s^{th} modal damping ratio, D_h is the parameter reflecting the damping mitigation effect on seismic response (Fu and Kasai 1998), and α is a coefficient that depends on earthquake type (JSSI 2013). In this paper, ξ_0 is defined

as 0.01, 0.02, 0.03, 0.05, 0.1, 0.15, 0.2, or 0.3, and α is defined as 25 or 75, depending on whether the response is compared to a suite of artificial or real ground motions.

The standard eigenvalue problem shown in Equation 19 is applied to complex eigenvalue analysis (Foss 1958). Note that the aim of this study is to evaluate the maximum seismic response, and the issue of time causality that arises when applying a Fourier or Hirbert transformation is neglected:

$$\begin{pmatrix} -\mathbf{M}^{-1}\mathbf{C} & -\mathbf{M}^{-1}\mathbf{K_{eq}} \\ \mathbf{I} & \mathbf{0} \end{pmatrix} \begin{Bmatrix} \lambda\{\varphi\} \\ \{\varphi\} \end{Bmatrix} = \lambda \begin{Bmatrix} \lambda\{\varphi\} \\ \{\varphi\} \end{Bmatrix} \tag{19}$$

where $\mathbf{I}$ is the unit matrix, $\mathbf{0}$ is the zero matrix, and $\{\varphi\}$ is the complex eigenvector.

VALIDATION

DATA SETS AND MODELING RULE

To confirm the accuracy and limitations of the GRSA routine, the calculated responses are compared to NLRHA using an implicit method (i.e., the Newmark beta method). One inherent limitation of GRSA is the reliance on initial coordinates, which ignores P-delta effects. While this is not expected to have a significant effect for drifts in the range of 1%–2%, geometric nonlinearity is included in the NLRHA by updating the coordinates related to the rotation matrix and the stiffness distribution using an updated Lagrangian incremental formulation.

A parametric validation study is conducted of regular 2-D frames with buckling-restrained braces (BRBs) used as EP dampers in single diagonal or chevron configurations. Schematic images are shown in Figure 4, and key structural properties listed in Table 2. In the 1- to 4-story models, a distributed mass is assigned only to the roof floor to remove the effects of higher modes. A range of yield ratios (i.e., achieved by adjusting the mass to produce a desired spectral displacement) is considered in these models. In the 8- to 64-story models, distributed mass is assigned to all stories in order to excite higher modes, and is

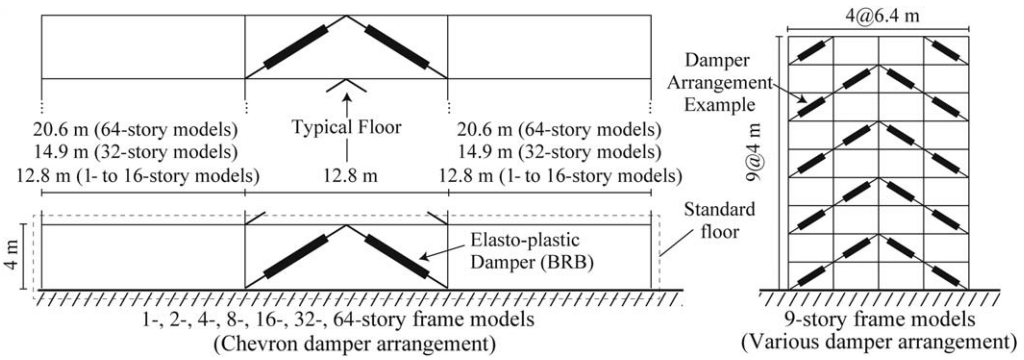

Figure 4. Schematic images of the 2-D frame models.

Table 2. Structural properties of 2-D frame models

Model series	No. stories (total height)	Damper arrangement	k_d/k_f	T (s) (1st mode)	Mass ratio of 1st mode	Max. μ
1-story frame	1 (4 m)	All	0.25	0.15–1.70	1.00	57.1
Low-rise frame	2 (8 m)	All	0.50	0.21–3.90	1.00	48.9
	4 (16 m)	Upper half	1.00	0.30–5.51		34.3
		Lower half	2.00			
Middle- to high-	8 (32 m)	All	4.00	0.62–2.35	0.68–0.90	8.8
rise frame	16 (64 m)	Upper half		1.33–4.52	0.67–0.87	9.5
	32 (128 m)	Lower half		2.96–8.03	0.66–0.85	10.1
	64 (256 m)			6.71–13.9	0.65–0.83	9.6
9-story frame	9 (36 m)	Various	1.00	1.00–1.27	0.73–0.88	3.7

adjusted so that the first natural period is equal to 0.03 times the building height (m) when k_d/k_f is 1.00. The ground motions applied include El Centro, Taft, JMA Kobe, and Hachinohe, spectrally matched to fit the Level 2 design response spectrum (approximately a 500-year event) of the Japanese building code. The initial viscous damping is set as a minimal 0.01 in the first and second modes to focus the response dependency on the EP damping, which is of primary interest. Note that the purpose of these models is to verify the accuracy of the proposed GRSA routine, and the maximum response is not always realistic. Conversely, a more realistic response was targeted for the 9-story models, which are used to study the effect of damper arrangements. This model is subjected only to the BCJ-L2 (Japanese artificial Level 2) wave, and the initial damping ratio is set as 0.02.

For simplicity, a single beam, column, and BRB size is used, and all connections are assumed to be rigid. The damper-to-moment frame stiffness ratio k_d/k_f is varied from 0.25 to 4.00 by adjusting the number of BRBs, and is calculated according to Equation 20:

$$k_d = 2\frac{A_b E}{L_b}\cos\theta_b, \quad k_f = n_c\frac{12EI_c}{L_c^3} \tag{20}$$

where k_d is the sum of the horizontal stiffness of the braces and k_f of the columns at a typical floor, n_c is the number of the columns, I_c is the column moment of inertia, and L_c is the column story height. The section area for all BRBs is set as $A_b = 3325\,\text{mm}^2$, assuming a 19×175 mm core. To concentrate the frame flexibility in the columns, the moment of inertia of the beams is set to 1,000 times that of the columns and rigid diaphragms modeled by setting the beam area to 1,000 times that of one column.

1-STORY FRAME MODELS

The accuracy is compared to NLRHA in Figure 5 for the 1-story models. Note that N in Figures 5 to 11 refers to the number of analysis runs (number of unique models $\times$ number of ground motion records). It was noted that the story drift ratio (SDR) was consistently overestimated when using GSM equivalent damping with the generalized RSA routine. This occurs because both the equivalent stiffness and complex

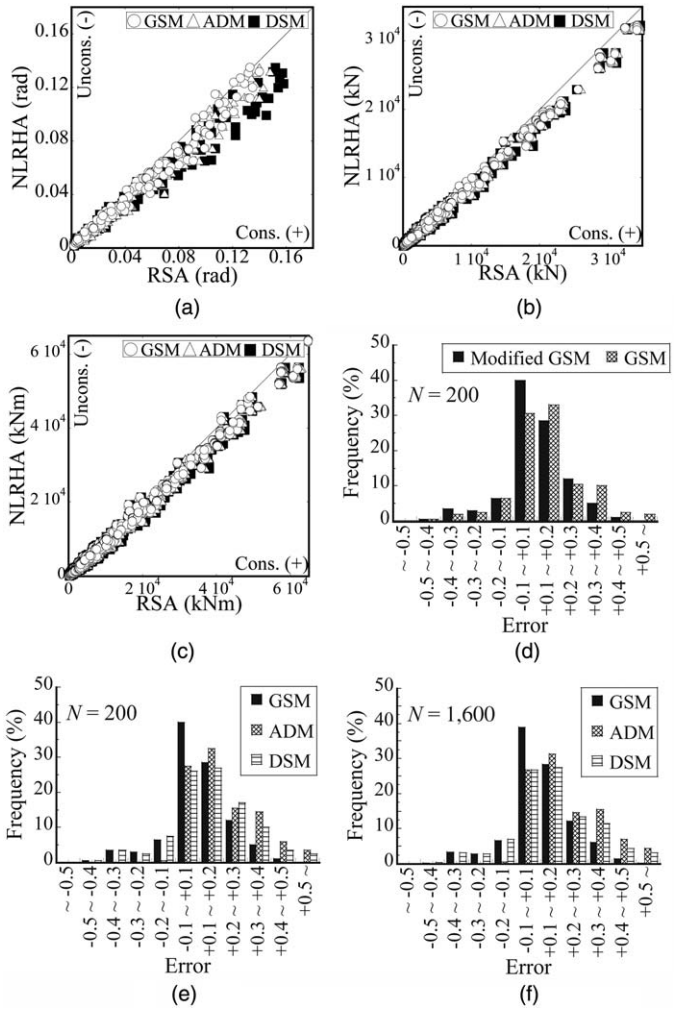

Figure 5. Comparison of NLRHA and generalized RSA in 1-story models: (a) SDR; (b) shear force; (c) bending moment; (d) SDR; (e) SDR; and (f) shear force.

damping ratio ξ' begin to decrease when the ductility μ exceeds approximately 8. Such values are unlikely to be of much practical relevance for normal design situations, but are nevertheless included in this study for comprehensive validation. To avoid this phenomenon, a modified GSM is used from here on, where the peak value of ξ' is used when the ductility is large, and the parameter b is defined as $2\gamma_K\xi'$. The improved accuracy is shown in Figure 5d, with the GRSA method achieving good agreement with NLRHA for a broad range of yield ratios, as shown in Figure 5a to 5c. Although GRSA with ADM equivalent damping is more conservative than with GSM, approximately 90% of responses have an error of −0.3 to +0.3 when using GSM, as shown in Figure 5e to 5f.

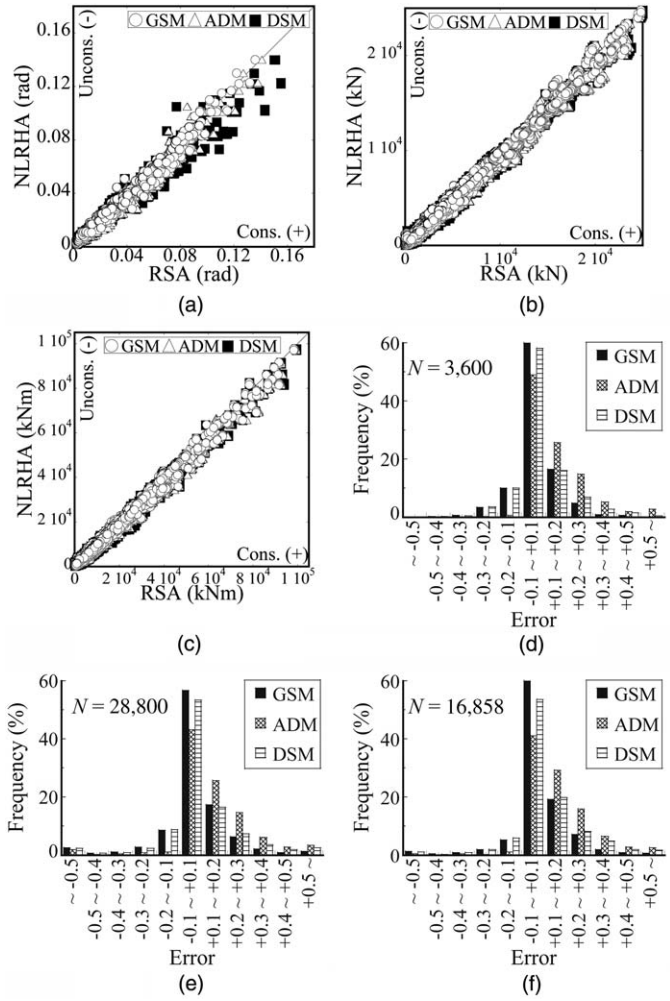

Figure 6. Comparison of NLRHA and generalized RSA in 2- and 4-story models: (a) SDR; (b) shear force; (c) bending moment; (d) SDR; (e) shear force; and (f) bending moment.

LOW-RISE FRAME MODELS

The accuracy of 2- and 4-story frame models is presented in Figure 6. As shown in Figure 6a to 6c, the response evaluation (even including the phase effects) agrees well with the NLRHA results. Moreover, Figure 6d to 6f show that either GSM or DSM is suitable for the computational response evaluation for a low-rise building where the first mode dominates, although ADM is generally recommended for conventional design procedures.

9-STORY FRAME MODELS INCLUDING VARIOUS DAMPER ARRANGEMENTS

A more realistic response considering various damper arrangements and dead loads is presented in Figure 7. The response evaluation, including deformation shapes and member

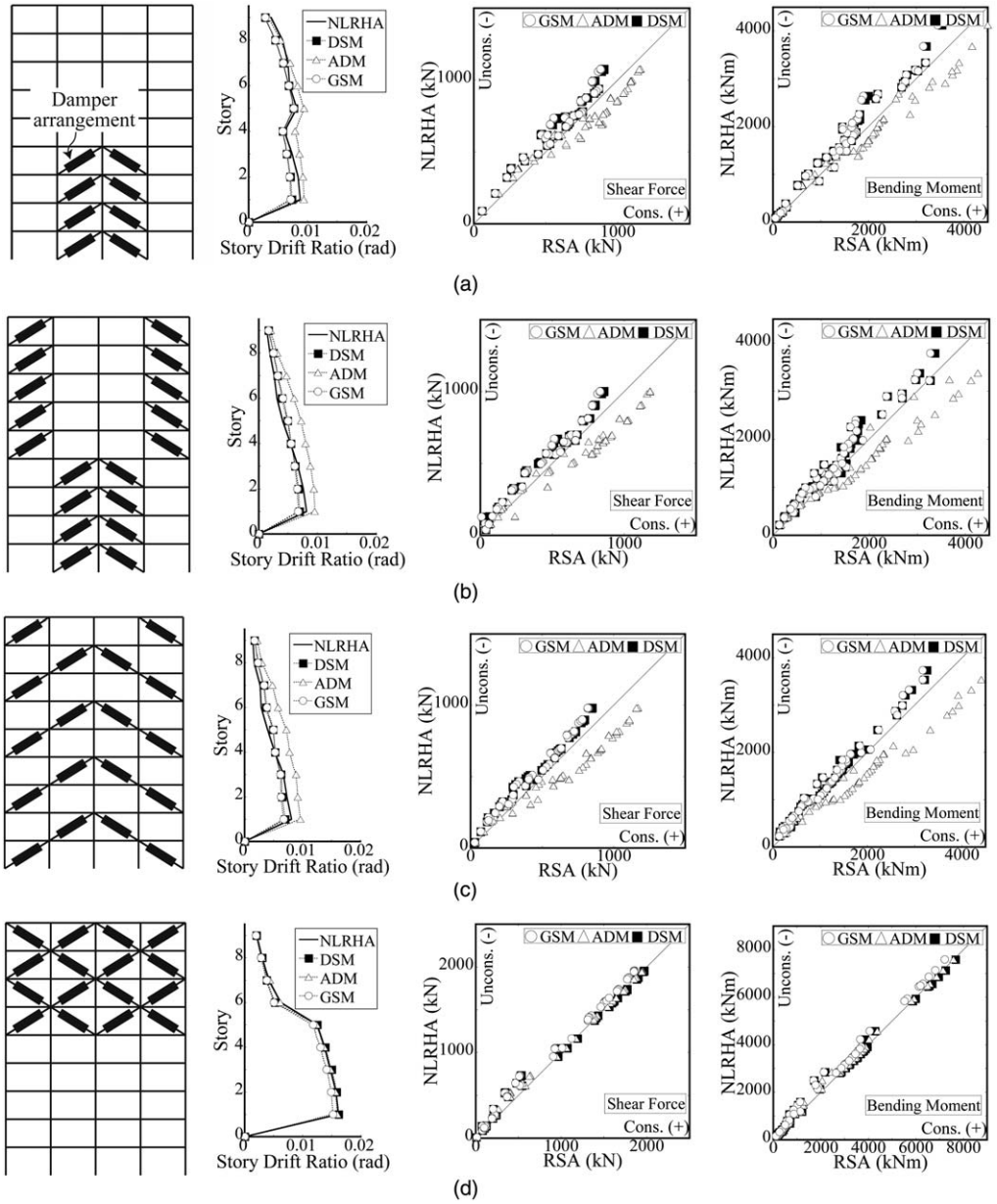

Figure 7. Comparison of NLRHA and generalized RSA for 9-story models: (a) Case 1; (b) Case 2; (c) Case 3; and (d) Case 4.

forces, corresponds well with the NLRHA results, and even has good agreement for arrangements producing less damping, such as the arrangement depicted in Figure 7d. In general, the accuracy of the GSM and DSM equivalent damping methods is better than that of ADM for the low-rise structures (≤9 stories), as shown in Figures 5 to 7.

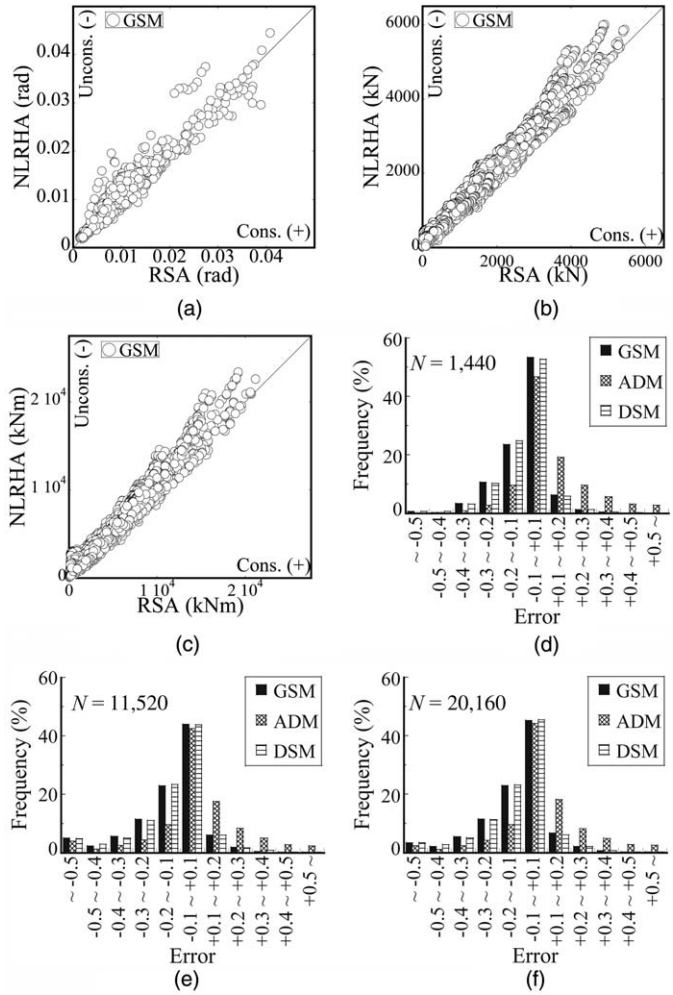

Figure 8. Comparison of NLRHA and generalized RSA in 8- and 16-story models. (a) SDR; (b) shear force; (c) bending moment; (d) SDR; (e) shear force; and (f) bending moment.

MIDDLE- TO HIGH-RISE FRAME MODELS

Figure 8 shows the accuracy for mid-rise buildings. Although the GSM and DSM errors are occasionally unconservative, approximately 80% of the responses produce member forces with errors of −0.3 to +0.2. In contrast with the GSM and DSM methods, the error distribution for ADM is consistently conservative, and is often more accurate than the other options.

Issues related to overall bending are often indicated in conventional design procedures (e.g., JSSI 2013), because the simplified lumped mass models forming the basis of these simple equations consider only shear deformations, and thus may overestimate the damper performance. An extreme example is shown in Figure 9, in which a small column area

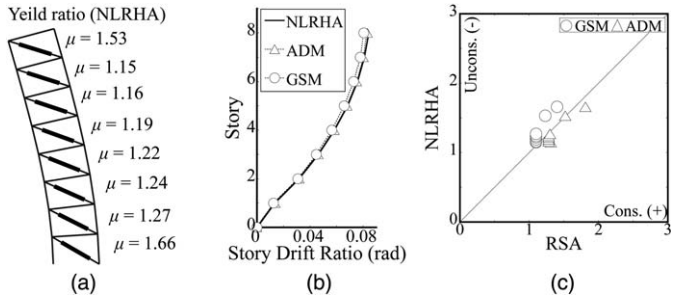

Figure 9. Comparison in the specific model to be cantilever bending (input: El Centro NS). (a) First mode shape; (b) SDR; and (c) yield ratio μ.

(set equal to brace area) is employed in order to intentionally excite overall bending deformations, and the k_d/k_f ratio set to 1.00. Because the GRSA method analyzes a frame, rather than a simplified lumped mass model, the effect of overall bending is accurately captured.

The accuracy for the high-rise models is presented in Figures 10 and 11, with the SDR response generally corresponding to the NLRHA results. The error distribution using the ADM equivalent damping method is better than when using GSM or DSM due to higher mode effects. Approximately 85% of plots using ADM have SDR errors within −0.3 to +0.2. Member forces are occasionally overestimated or underestimated by a large margin, especially for taller 64-story models, but, nevertheless, about 80% of responses have errors within −0.3 to +0.1 when using ADM. Those with larger errors appear to be affected by geometric nonlinearity, as P-delta effects are far more significant for high-rise frames as compared to shorter buildings (≤16 stories). Nevertheless, this study suggests that the GRSA provides a sufficiently accurate estimation of the displacements for high-rise buildings with heights up to 200 m.

EXAMPLE APPLICATION TO A 3-D STRUCTURE

To illustrate the type of structures where the proposed method could be usefully applied, an example 3-D truss tower retrofitted with VE, and then EP, dampers is presented. This structure was constructed in Japan as a telecommunications tower and seismically retrofitted with BRBs. The as-built EP damper arrangement and sizes are shown in Figure 12, as well as a VE damper scheme that was previously generated using a genetic algorithm (Takeuchi et al. 2015). The seismic input is Hachinohe EW, spectrally matched to the Japanese Level 2 design spectrum, which is amplified according to the site ground conditions. The dominant modes used in the generalized RSA are selected to achieve a 90% mass ratio according to Equation 21, and α is defined as 25 in the damping response reduction equation (Equation 18).

$$\{1\}^{\mathrm{T}}\mathbf{M}\{1\} = \{1\}^{\mathrm{T}}\mathbf{M}\mathrm{Re}(\mathbf{U}\boldsymbol{\lambda}\boldsymbol{\beta}) = \sum_{s=1}^{r} M_s = const., \;\; M_s = 2 \times \{1\}^{\mathrm{T}}\mathbf{M}\mathrm{Re}(\lambda_s\beta_s\{\varphi_s\}) \quad (21)$$

where r is the size of the mass matrix, $\mathbf{U}$ is the $r \times 2r$ modal matrix for the complex eigenvector, $\boldsymbol{\lambda}$ is the $2r \times 2r$ diagonal matrix of the complex eigenvalues, and $\boldsymbol{\beta}$ is the vector of

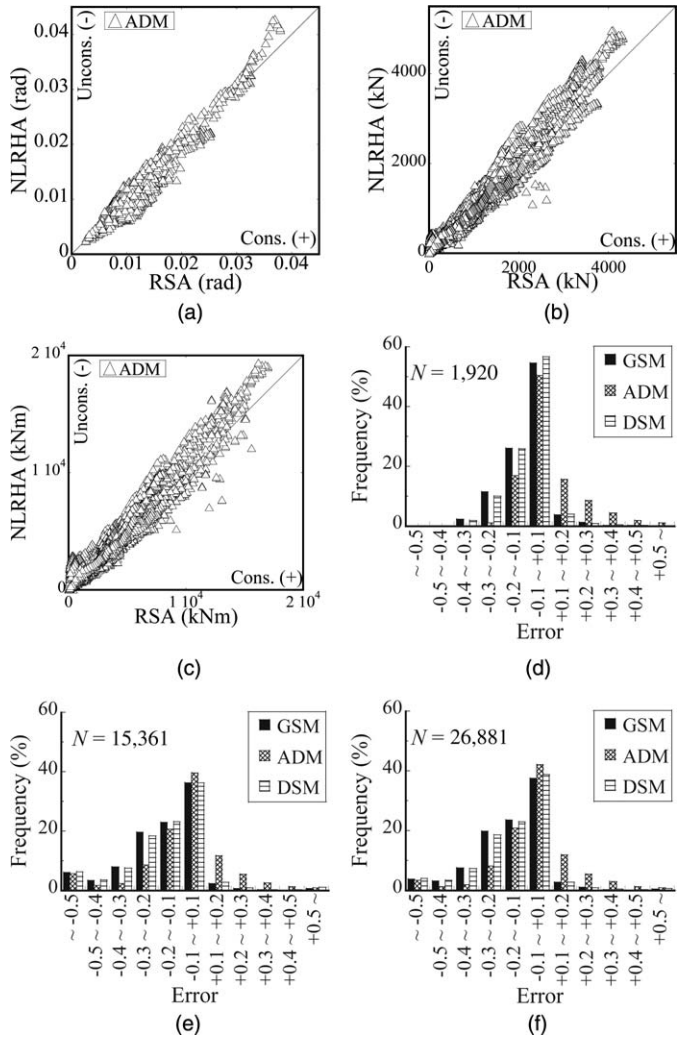

Figure 10. Comparison of NLRHA and generalized RSA for 32-story models. (a) SDR; (b) shear force; (c) bending moment; (d) SDR; (e) shear force; and (f) bending moment.

the complex participation factors. Note that the conjugate pairs are alternatingly arranged in the rows or columns of $\mathbf{U}$, $\boldsymbol{\lambda}$, and $\boldsymbol{\beta}$.

A comparison of the GRSA and NLRHA is shown in Figure 13. For the VE model, the error in roof displacement is +7% using the GRSA method, which is about half the +13% error of the extended equivalent linear approach used in the original analysis. For the EP model, the GRSA has excellent agreement with the NLRHA results, accurately tracking the distribution and magnitude of drift of the 3-D model. The dominant modes and modal mass ratios for the EP model are shown in Figure 14, indicating that higher modes (i.e., the seventh and ninth modes) are predominant. This results in the ADM method

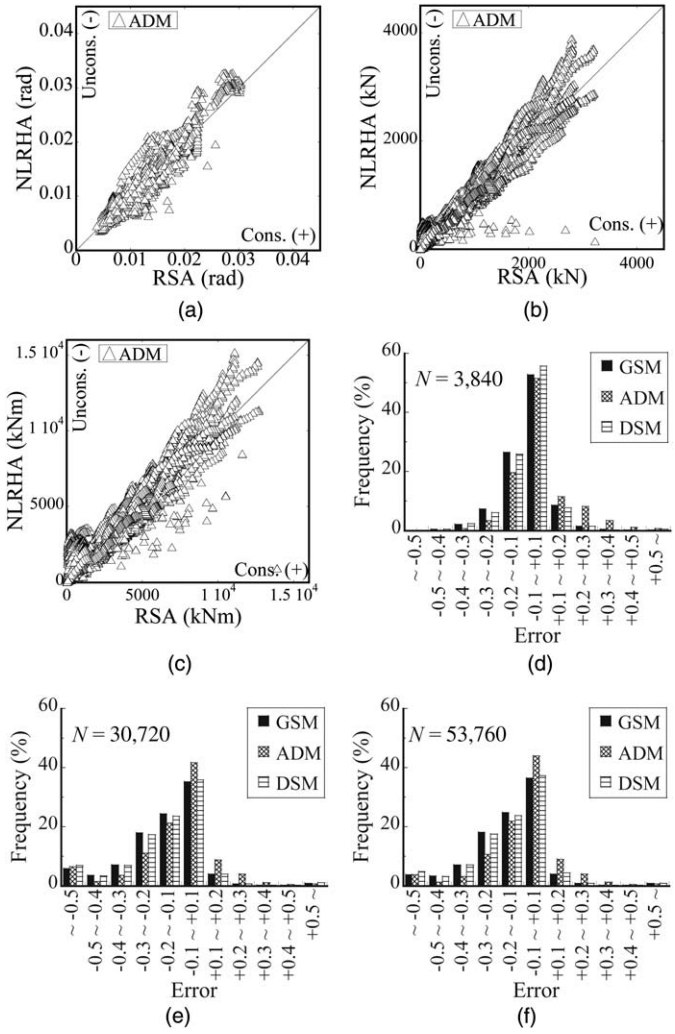

Figure 11. Comparison of NLRHA and generalized RSA for 64-story models. (a) SDR; (b) shear force; (c) bending moment; (d) SDR; (e) shear force; and (f) bending moment.

providing a better estimate than the GSM or DSM methods, which is consistent with the findings for the high-rise structures.

Even for this relatively simple structure, the number of DOFs is 810. NLRHA of the EP model took approximately 33 min to run, while the GRSA with ADM took approximately 12 s. A local desktop computer was used with an Intel Core i7 including six processors (3.6 GHz) and DDR4-2400 memory (32 GB), similar to that available to design engineers. The code was compiled and optimized using Intel Fortran, and was written by the first author using Fortran 90/95, with the exception of some numerical libraries.

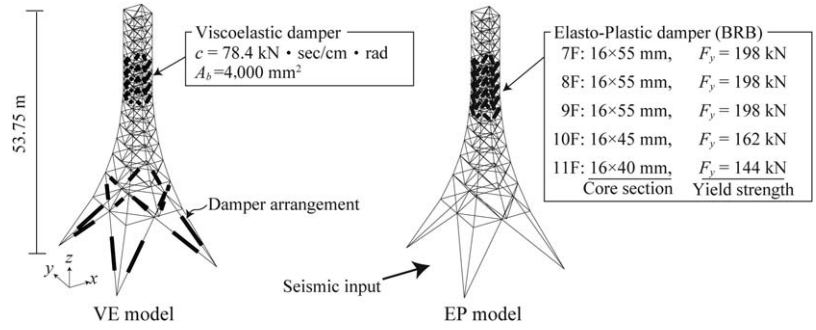

Figure 12. Schematic image of truss tower models.

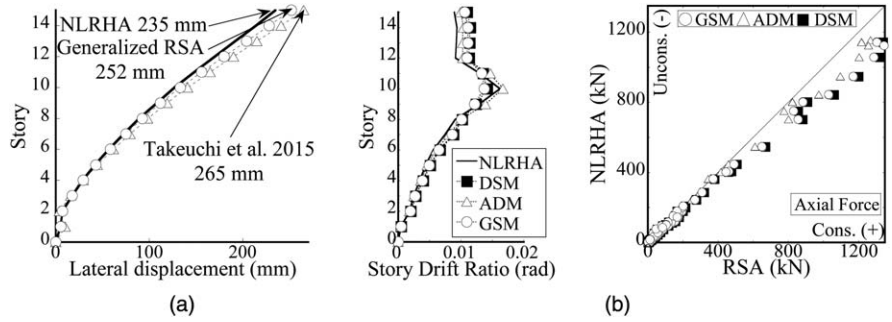

Figure 13. Comparison of the response evaluation and NLRHA results: (a) VE model and (b) EP model.

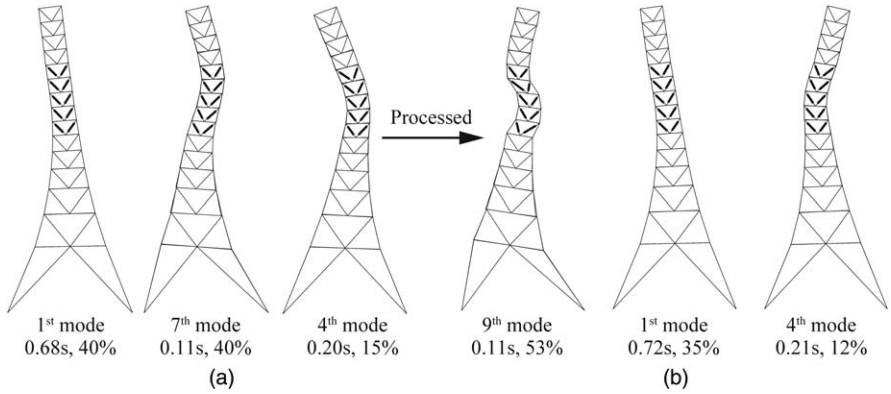

Figure 14. Shift in mode shapes of EP model using ADM (caption: natural period, mass ratio): (a) Initial mode shapes and (b) final complex mode shapes.

CONCLUSIONS

In this study, a GRSA routine was developed. This method is capable of analyzing frame models with supplementary dampers, with displacement dependent EP damping incorporated as complex stiffness and a proposed modified CQC method, extending the work of Sinha and Igusa (1995). The validity of the GRSA was confirmed through comparison to NLRHA. The following conclusions can be drawn:

1. The maximum seismic response for complex asymmetric damped systems can be evaluated using a proposed modified CQC method. This is based on the eigenvalue expression of a SDOF model and includes both viscous and EP damping, the latter as complex stiffness. A 3-D element matrix is proposed that includes a complex axial stiffness term, and is confirmed to provide a good estimate of displacement-dependent damping of brace and axial members, such as BRBs.
2. Several methods were studied for the required equivalent damping expression. A modified GSM and DSM method was found to be most accurate for structures where the first mode is dominant. However, the ADM is consistently more conservative than other methods, and is most accurate for structures with significant higher mode participation.
3. Numerical validation studies of 2-D frame models, which consisted of diagonal braces and an elastic moment frame, indicated good agreement with the NLRHA results, particularly for low- and mid-rise frames ($\leq$16 stories). Approximately 80% of the model responses predicted the peak SDR, shear force, and bending moment with errors of −0.3 to +0.2. In contrast, the accuracy in predicting the member forces decreased for high-rise buildings due to global P-delta effects, while the accuracy of story drifts (SDR) was generally maintained.
4. An example of the GRSA method to a 3-D truss tower structure retrofitted with BRBs was presented. The proposed method proved comparably accurate to NLRHA, while requiring only a small fraction of the time.

The energy-dissipation devices discussed in this study include linear viscous, linear VE, and EP dampers. Nonlinear viscous and nonlinear VE dampers may also be considered by adjusting the phase when updating the damping matrix, using an equivalent linearized element (e.g., Voigt model) and applying equivalent linear approaches for frequency-dependent damping, which have been proposed in previous studies.

REFERENCES

Architecture Institute of Japan (AIJ), 2016. *Design Recommendations for Seismically Isolated Buildings*, Maruzen Publishing Co., Tokyo, 210 pp.

Bae, S., Jeong, W. B., and Cho, J., 2014. Transient response of complex stiffness system using a green function from the Hilbert transform and the steady space technic, in *Proceedings, The 43rd International Congress on Noise Control Engineering*, 16–19 November 2014, Melbourne, Australia, 10.

Biggs, J. M., and Whitman, R. V., 1970. Soil structure interaction in nuclear power plants, in *Proceedings, The 3rd Japanese Earthquake Engineering Symposium*, 17–20 November 1970, Tokyo, Japan, 89–95.

Caughey, T. K., 1960. Sinusoidal excitation of a system with bilinear hysteresis, *Journal of Applied Mechanics* **27**, 640–643.

Eatherton, M. R., Ma, X., Krawinkler, H., Deierlein, G. G., and Hajjar, J. F., 2014. Quasi-static cyclic behavior of controlled rocking steel frames, *Journal of Structural Engineering* **140**, 04014083-1–04014083-11.

Foss, K. A., 1958. Coordinates which uncouple the equation of motion of damped linear dynamic systems, *Journal of Applied Mechanics* **32**, 361–364.

Fu, Y., and Kasai, K., 1998. Comparative study of frames using viscoelastic and viscous dampers, *Journal of Structural Engineering* **124**, 514–522.

Huang, B., and Takeuchi, T., 2017. Dynamic response evaluation of damped-outrigger systems with various heights, *Earthquake Spectra* **33**, 665–685.

Ishimaru, S., and Chunhuan, K., 2015. New version / ductility factor control method - Evaluation of optimal viscous damping ratios and cumulative ductility factors for a structure with specified ductility factor, *Journal of Structural and Construction Engineering*, Architecture Institute of Japan (AIJ) **80**, 241–251 (in Japanese).

Jacobsen, L. S., 1930. Steady forced vibration as influenced by damping, *Transaction of the American Society of Mechanical Engineers* **51**, 169–181.

Jacobsen, L. S., 1960. Damping in composite structures, in *Proceedings, The 2nd World Conference on Earthquake Engineering*, 11–18 July 1960, Tokyo, Japan, 1029–1043.

Japan Society of Seismic Isolation (JSSI), 2013. *Manual for Design and Construction of Passively-Controlled Buildings*, 3rd Edition, Daioh Co., Ltd., Tokyo, 561 pp.

Jennings, P. C., 1968. Equivalent viscous damping for yielding structures, *Journal of the Engineering Mechanics Division* **94**, 103–116.

Kasai, K., Ito, H., Motoyui, S., Ozaki, H., Ishii, M., Kajiwara, K., and Hikino, T., 2009. Full-scale tests on value-added performance of 5-story building with various dampers commercially available, in *Proceedings, The 3rd International Conference on Advances in Experimental Structural Engineering*, 15–16 October 2009, San Francisco, CA.

Myclestad, N. O., 1952. The concept of complex damping, *Journal of Applied Mechanics* **19**, 284–286.

Newmark, N. M., and Rosenblueth, E., 1971. *Fundamentals of Earthquake Engineering*, Prentice-Hall Inc., Ch. **11**, 321–363.

Ookouchi, Y., Takeuchi, T., Uchiyama, T., Suzuki, K., Sugiyama, T., Ogawa, T., and Kato, S., 2005. Experimental studies of tower structures with hysteretic dampers, in *Proceedings, International Symposium on Shell and Spatial Structures*, 6–10 September 2005, Bucharest, Romania, 8.

Shibata, A., and Mete, S., 1976. Substitute-structure method for seismic design in R/C, *Journal of the Structural Division*, ASCE **102**, 1–18

Sinha, R., and Igusa, T., 1995. CQC and SRSS methods for non-classically damped structures, *Earthquake Engineering and Structural Dynamics* **24**, 615–619.

Shirai, K., and Inoue, N., 2014. A seismic response estimation method for RC structures using random vibration theory, *Journal of Advanced Concrete Technology* **12**, 62–72.

Takeuchi, T., Chen, X., and Matsui, R., 2015. Seismic performance of controlled spine frames with energy-dissipating members, *Journal of Constructional Steel Research* **114**, 51–65.

Takeuchi, T., Kinouchi, Y., Matsui, R., and Ogawa, T., 2015. Optimal arrangement of energy-dissipating members for seismic retrofitting of truss structures, *American Journal of Engineering and Applied Sciences* **8**, 455–464.

Warburton, G. B., and Soni, S. R., 1977. Errors in response calculations for non-classically damped structures, *Earthquake Engineering and Structural Dynamics* **5**, 365–376.

(Received 22 September 2017; accepted 21 March 2018)